

# Phase behavior of a symmetrical binary fluid mixture

Jürgen Köfner<sup>1</sup>, Nigel B. Wilding<sup>2</sup>, and Gerhard Kahl<sup>3</sup>

<sup>1</sup> Faculty of Physics, University of Vienna, Boltzmannngasse 5, A-1090 Wien, Austria

<sup>2</sup> Department of Physics, University of Bath, Bath BA2 4LP, United Kingdom

<sup>3</sup> Center for Computational Materials Science and Institut für Theoretische Physik, TU Wien, Wiedner Hauptstraße 8-10, A-1040 Wien, Austria

(Dated: September 24, 2018)

We have investigated the phase behaviour of a symmetrical binary fluid mixture for the situation where the chemical potentials  $\mu_1$  and  $\mu_2$  of the two species differ. Attention is focused on the set of interparticle interaction strengths for which, when  $\mu_1 = \mu_2$ , the phase diagram exhibits both a liquid-vapor critical point and a tricritical point. The corresponding phase behaviour for the case  $\mu_1 \neq \mu_2$  is investigated via integral-equation theory calculations within the mean spherical approximation (MSA), and grand canonical Monte Carlo (GCMC) simulations. We find that two possible subtypes of phase behaviour can occur, these being distinguished by the relationship between the critical lines in the full phase diagram in the space of temperature, density, and concentration. We present the detailed form of the phase diagram for both subtypes and compare with the results from GCMC simulations, finding good overall agreement. The scenario via which one subtype evolves into the other, is also studied, revealing interesting features.

## I. INTRODUCTION

As one proceeds from a simple single component fluid to a binary mixture, the complexity of the phase behaviour increases dramatically. The range of possible behavior was first summarized on a qualitative level more than 25 years ago in the seminal study of van Konynenburg and Scott [1]. Using a simple mean-field (MF) ansatz for the equation-of-state, these authors found that in binary mixtures the additional thermodynamic degree of freedom in the form of the concentrations of the two species,  $c_1$  and  $c_2$ , with  $c \equiv c_1 = 1 - c_2$  (or, alternatively, the difference in the chemical potentials of the two species,  $\Delta\mu = \mu_1 - \mu_2$ ), considerably widens the spectrum of possible features [2]. Among these are upper and lower critical points, tricritical points, critical end points (CEPs), quadruple (i.e., four phase) points, lines of critical points, or triple lines. The details of which features actually emerge in practice for a given model, and in which order (i.e., the phase diagram topology), were found to depend in a non-trivial manner on the precise combination of interparticle interaction parameters, i.e., three energy parameters  $\epsilon_{ij}$  and three length scales  $\sigma_{ij}$  (with  $i, j = 1, 2$ ), together with parameters that characterize the range of the attractive interactions.

Today, more than a quarter of a century later, both liquid state theories [3] and computer simulations [4, 5] offer standards of accuracy that greatly surpass those obtainable from MF-based theories. It therefore seems appropriate to reconsider the schematic overview of phase diagram topologies provided by van Konynenburg and Scott [1], at a more *quantitative* level. The present contribution aims to take a step in this direction. However, owing to the high-dimensional space of interaction parameters, one is necessarily restricted to a particular model. In the interests of numerical tractability, we have chosen to consider a *symmetrical* binary mixture. In such a system, the interactions between particles of like species are equal, i.e.,  $\Phi_{11}(r) = \Phi_{22}(r) = \Phi(r)$ , while the interactions between unlike species are related via  $\Phi_{12}(r) = \delta\Phi(r)$ . Thus for a prescribed form of interaction potential,  $\Phi(r)$ , the phase behaviour is controlled by the single parameter  $\delta$ . Since for the case  $\delta > 1$ , such a system exhibits only a simple liquid-vapour (LV) transition, we focus here on the more interesting case of  $\delta < 1$ , where the competition between a LV on the one hand, and a demixing transition (into phases of generally different concentrations), gives rise to a rather rich phase behaviour. For the reasons explained below, we will focus on a mixture where  $\Phi(r)$  takes the form of a hard-core plus attractive Yukawa (HCY) interaction; nevertheless we anticipate that any other similar forms of potential (such as Lennard-Jones or square-well potentials) will lead to results qualitatively similar to those we present.

In recent years, numerous authors have investigated the phase diagram of symmetrical binary mixtures using liquid state theories (of varying degrees of sophistication), as well as computer simulations [6, 7, 8, 9, 10, 11, 12, 13, 14, 15, 16, 17, 18, 19, 20, 21, 22, 23]. However, these studies have been confined for the large part to the special case of equimolar concentrations of the two species (i.e., for  $\Delta\mu = 0$ ). The resulting picture of the phase behaviour shows four distinct topologies (or archetypes) of phase diagram as  $\delta$  is varied. Starting at  $\delta = 1$ , and in order of decreasing  $\delta$ , these are distinguishable as follows: in the first type, the critical line that characterizes the demixing transition (the so-called  $\lambda$ -line) intersects the LV coexistence line at liquid densities and at temperatures well below the LV critical temperature, forming a critical end point (CEP); in the second type, the  $\lambda$ -line approaches LV coexistence again from the liquid side, but slightly below the LV critical temperature, terminating in a separate tricritical point which itself marks the end of a first order transition between mixed and demixed liquid phases; in the third type the

$\lambda$ -line intersects the LV critical point directly, the two combining to form a tricritical point. Finally in the fourth type the  $\lambda$ -line intersects the low density branch of the LV coexistence curve, forming a CEP. For clarity we summarize in Table I the various notations that have been introduced in literature to classify the phase diagrams of binary symmetrical mixtures for  $\Delta\mu = 0$ . A schematic presentation of the first three types can be found in Fig. 1 of [13], while the fourth type is shown in Fig. 1 of [22]. We note that in analytical calculations the precise value of  $\delta$  marking the boundaries between two successive types for a particular interaction potential, depends to some extent on the method used for the calculation.

For the more general case of non-equimolar concentrations (i.e., allowing for  $\Delta\mu \neq 0$ ), relatively few investigations of the phase behaviour can be found in literature [14, 19, 24]. This fact undoubtedly reflects the obstacles encountered by both simulation and theoretical approaches in dealing with the increased complexity of the full phase diagram spanned by temperature  $T$ , pressure  $p$ , and the chemical potential difference  $\Delta\mu$ . Probably the first study to provide a rough idea of the complexity of the full phase diagram was that of Antonyevich *et al.* [14], based on conventional integral-equation techniques. It was followed shortly afterwards by the remarkable study of Pini *et al.* [19], who used the highly accurate Hierarchical Reference Theory (HRT) [25], complemented by MF calculations, to provide the first insight into the complex topology of the *full* phase diagram of binary symmetrical mixtures for  $\Delta\mu \neq 0$ . However, the high computational costs of HRT did not permit a systematic discussion of the topology of the phase diagram.

In this work we present a systematic investigation of the full phase diagram for one of the archetypes of phase diagram outlined above, namely that exhibiting both a LV critical point and a first order liquid-liquid transition terminating at a tricritical point [27]. Our investigations are based on the mean spherical approximation (MSA) and grand canonical Monte Carlo (GCMC) simulations. We have chosen MSA for the simple reason that for a mixture of HCY fluids it provides closed (i.e., semi-analytic) expressions for the structural and the thermodynamic properties [28]; these concern in particular the pressure,  $p$ , and the chemical potentials,  $\mu_1$  and  $\mu_2$ . The formalism for a general mixture of HCYs is summarized in [29]. Using then MATHEMATICA<sup>TM</sup> [30], the solution of the coexistence equations is considerably less involved than it is the case for integral-equation theories that have to be solved fully numerically [3]. Although MSA is less accurate (in particular in the critical regions) than, e.g., advanced liquid state theories, such as HRT [25] or the self-consistent Ornstein-Zernike approximation (SCOZA) [18, 21, 31], it is nevertheless able to provide results of reasonable accuracy; this will also be corroborated in the present contribution. GCMC, when used in combination with extended sampling and histogram reweighting techniques provides a powerful means of studying fluid phase equilibria with a precision which is limited only by statistical errors [13, 32]. We extend its use here to the case of a chemical potential difference field, thus providing a benchmark against which to test the MSA results.

Our work makes progress on two fronts. First, we demonstrate that liquid state theories and computer simulations have reached levels of accuracy and efficiency that the full phase diagram [i.e., in  $(T, \rho, c)$ - or in  $(T, p, \Delta\mu)$ -space] of a symmetrical binary fluid mixture can be determined on a semi-quantitative level. We note that even a few years ago such an aim was considered to be too ambitious [19]. Second, we show that our simple model exhibits a wider spectrum of topologies of phase behaviour than one might have expected from previous investigations, in particular from those that were restricted to the equimolar case. Specifically, we confirm that for the archetype of phase behaviour considered (whose associated domain of  $\delta$  is defined on the basis of the  $\Delta\mu = 0$  phase diagram topology), two distinct subtypes emerge when one considers  $\Delta\mu \neq 0$ , as already suggested by Pini *et al.* [19] on the basis of selected isothermal cuts through the phase diagram. Our exposition of the *full* phase diagram sheds further light on the nature of the subtypes, by showing that their topologies are defined by the location of four coexistence surfaces (each of which carries a critical line), which intersect in four triple lines. Some of these triple lines do not originate at the  $\lambda$ -line at equal concentrations. We consider the locus of the triple lines to be the key quantities that distinguish the two subtypes of phase behaviour. We discuss in detail the transition scenario between the two subtypes, which has not yet been documented in literature and which reveals new and interesting details about the critical behaviour of the system. The existence of the two subtypes is confirmed by the results of the GCMC simulation studies which, while being less comprehensive than the theoretical ones, demonstrate that simulation can be predictive regarding quite subtle features of the phase diagram.

Although a binary symmetrical mixture might at first sight seem to be a system of purely academic interest, arguments have been put forward in literature that they are able to reflect features of realistic systems: van Konynenburg and Scott [1] note that ‘the only real binary systems in which such symmetry occurs are mixtures of  $d, l$ -optical isomers [33]’, while Woywod and Schoen [24] find that the phase behaviour of  $^3\text{He}$ - $^4\text{He}$  mixtures contains many features of the topology of the phase diagram of binary symmetrical mixtures. Furthermore, as we shall discuss later, the symmetrical mixture has direct relevance to some classes of spin fluid models.

The paper is organized as follows. In Sec. II A, we introduce our model, a symmetrical binary fluid mixture in which particles interact via the HCY potential. The MSA integral-equation strategy is then outlined, as is the grand canonical simulation methodology. Sec. III represents in turn our MSA and GCMC results for the phase behaviour of the system for non-zero chemical potential difference field. Finally in Sec. IV, we attempt to set our results within their wider context, and assess the outlook for future work.

## II. MODEL AND METHODS

### A. The model

We consider a binary symmetrical mixture where the particles interact via the HCY potential

$$\Phi_{ij}(r) = \begin{cases} \infty & r \leq \sigma \\ -\epsilon_{ij}\sigma\frac{1}{r}\exp[-z(r-\sigma)] & r > \sigma \end{cases} . \quad (1)$$

Here the  $\epsilon_{ij}$  are the contact values of the potentials,  $\sigma$  is the hard-core diameter, and  $z$  is the inverse screening length, assigned the value  $z\sigma = 1.8$  in this work. Further the system is characterized by a temperature  $T$  [with  $\beta = (k_B T)^{-1}$ ] and a number density  $\rho = N/V$ ,  $N$  being the total number of particles in a volume  $V$ . Defining  $c$  as the concentration of species 1, we introduce partial number densities  $\rho_1 = c\rho$  and  $\rho_2 = (1-c)\rho$ ; in the expressions below we use  $x_1 = c$  and  $x_2 = 1-c$ . Standard reduced units will be used throughout the paper.

### B. Mean spherical approximation

The solution of the Ornstein-Zernike equations [3] along with the MSA closure relation, i.e.,

$$\begin{aligned} c_{ij}(r) &= -\beta\Phi_{ij}(r) & r > \sigma \\ g_{ij}(r) &= 0 & r \leq \sigma \end{aligned} \quad (2)$$

can be carried out for this particular system to a large extent analytically [28]. Here the  $c_{ij}(r)$  and the  $g_{ij}(r)$  are the direct correlation functions and the pair distribution functions, respectively. Our solution strategy is based on the general formalism presented by Arrieta *et al.* [29] for the MSA solution of multi-component HCY systems. These authors have derived a set of coupled, non-linear equations for the initially unknown coefficients that characterize the correlation functions  $c_{ij}(r)$ . These equations require a fully numerical solution (see below); for details we refer the interested reader to ref. [29]. Once these coefficients are obtained, essentially all thermodynamic properties can be calculated via simple algebraic expressions. Below we present only those that we require for the present contribution.

Within the MSA the thermodynamic properties derived via the energy route are usually more accurate than via other routes [34]. In the following, we list expressions for the excess (over the hard-sphere (HS) reference system) pressure and chemical potentials. The corresponding properties of the reference system are given by the Carnahan-Mansoori-Starling-Leland (CMSL) equation of state [35]. With  $p_E = p_E^{\text{CMSL}} + \Delta p_E$  and  $\mu_i = \mu_i^{\text{CMSL}} + \Delta\mu_i$  ( $i = 1, 2$ ), these quantities are given by

$$\frac{\beta p^{\text{CMSL}}}{\rho} = \frac{1}{1-\eta} + \frac{18(\xi_1\xi_2 + \xi_2^2)}{\pi\rho(1-\eta)^2} + \frac{6\eta\xi_2^3}{\pi\rho(1-\eta)^3} \quad (3)$$

$$\frac{\beta\Delta p_E}{\rho} = \frac{\pi}{3}\rho \sum_{ij} x_i x_j \sigma^3 \{[g_{ij}(\sigma)]^2 - [g_{ij}^0(\sigma)]^2\} + J \quad (4)$$

$$\begin{aligned} \beta\mu_i^{\text{CMSL}} &= \ln\left(\frac{\rho_i}{1-\eta}\right) + \frac{\frac{\pi}{6}\rho\sigma^3 + 3\sigma\xi_2 + 3\sigma^2\xi_1}{1-\eta} + \\ &+ \frac{3\sigma^3\xi_1\xi_2 + 3\sigma^3\xi_2^2}{(1-\eta)^2} + \frac{3\sigma^2\xi_2^2}{\eta(1-\eta)^2} + \\ &+ \frac{3\sigma^2\xi_2^2 \ln(1-\eta)}{\eta^2} - \frac{(\sigma^3\xi_2^3)(2-5\eta+\eta^2)}{\eta^2(1-\eta)^3} + \\ &- \frac{2\sigma^3\xi_2^3 \ln(1-\eta)}{\eta^3} \end{aligned} \quad (5)$$

$$\beta\Delta\mu_i = -\frac{2\pi}{z} \sum_j \rho_j K_{ij} G_{ij} - \frac{1}{2} \sum_j \rho_j [\tilde{c}_{ij}(0) - \tilde{c}_{ij}^0(0)] \quad (6)$$

where  $\xi_j = \pi/6(\rho\sigma^j)$ ,  $j = 1, 2, 3$ ; in particular  $\xi_3 = \eta$ , the packing fraction. Further parameters that appear in these relations (such as  $J$ ,  $G_{ij}$ , and  $K_{ij}$ ) are *a priori* unknown quantities, which are obtained from the numerical solution of the non-linear equations mentioned above. The  $g_{ij}(\sigma)$  and the  $g_{ij}^0(\sigma)$  are the values of the pair distribution functions of the HCY and of the HS reference system at contact. Finally,  $\tilde{c}_{ij}(0)$  and  $\tilde{c}_{ij}^0(0)$  are the zero-components of the Fourier-transform of the direct correlation functions for the HCY and the HS system. Details of the numerical solution of the MSA which leads to the full phase diagram will be presented in the Appendix.

### C. Computer simulations

Many features of the simulation techniques employed in the present study have previously been detailed elsewhere [11, 13, 32]. Accordingly, we confine the description of our methodology to its essentials, except where necessary to detail a new aspect.

GCMC simulations were performed using a standard Metropolis algorithm [13, 36]. The simulation scheme comprises two types of operations:

1. Particle insertions and deletions.
2. Particle identity transformations:  $1 \rightarrow 2$ ,  $2 \rightarrow 1$ .

Since particle positions are sampled implicitly via the random particle transfer step, no additional particle translation moves are required. Indeed it is the sampling of density fluctuations which represent the bottleneck for this problem, and the incorporation of particle translations does nothing to improve sampling efficiency.

The simulations were performed using the potential of eq. (1), truncated at  $r_c = 3.0\sigma$ . A mean-field long range correction for the effects of this truncation was applied in the usual manner [4]. To minimize the overheads associated with identification of neighbor interactions, we employed a cell decomposition scheme [36]. This involves partitioning the periodic simulation space of volume  $L^3$  into  $l^3$  cubic cells, each of linear dimension of the interaction range, i.e.,  $L/l = 3.0$ . We chose to study system sizes corresponding to  $l = 4$ ,  $l = 7$ , and  $l = 9$ . The smallest system size was used to trace phase boundaries away from critical points; additionally, the larger ones were employed near criticality to facilitate crude finite-size scaling estimates of critical point locations. At each state point, equilibration periods of up to  $2 \times 10^3$  MCS (Monte Carlo sweeps, where one sweep comprises  $l^3$  attempted transfers and identity swaps) were used. Sampling frequencies were 500 MCS for the  $l = 4$  system size rising to 2000 MCS for the  $l = 9$  system. The total number of samples drawn for each state point studied was about  $10^6$ .

In this work we explore the parameter space spanned by the variables  $(\mu_1, \Delta\mu, T, \delta)$ . To accomplish this, without having to perform a very large number of simulations, we employed the histogram reweighting technique [37]. Use of this technique permits histograms obtained at one set of model parameters to be reweighted to yield estimates corresponding to another set of model parameters. To enable simultaneous reweighting in all four fields  $(\mu_1, \Delta\mu, T, \delta)$ , one must sample the conjugate observables  $(\rho_1, \rho_1 - \rho_2, u, u_d)$ , with  $\rho_1 = N_1/V$ ,  $\rho_2 = N_2/V$ ,  $u$  the configurational energy density, and  $u_d$  that part of  $u$  associated with interactions between *dissimilar* particle species. These quantities were accumulated in the form of a list during the simulations, and histograms of their forms were created and reweighted via post-processing of the entries in the list.

Within a region of first order coexistence, a standard grand canonical ensemble scheme is severely hampered by the large free energy barrier separating the two coexisting phases. This barrier leads to metastability effects and prohibitively long correlation times. To circumvent this difficulty, we have employed the multicanonical preweighting method [38] which enhances sampling of the interfacial configurations of intrinsically low probability. This is achieved by incorporating a suitably chosen weight function in the GCMC update probabilities. The weights are subsequently ‘folded out’ from the sampled distributions of observables to yield the correct Boltzmann distributed quantities. Use of this method permits the direct measurement of the distribution of observables at first order phase transitions, even when these distributions span many decades of probability. Details concerning the implementation of the techniques can be found in references [38, 39].

Phase boundaries were traced in the space of  $(\mu_1, \Delta\mu, T)$  by applying the equal peak weight criterion [40] to the distribution of the appropriate fluctuating order parameter, whether this be the concentration or the overall density. Critical point parameters were estimated using a crude version of the finite-size scaling (FSS) analysis described in ref.

[32]. The analysis involves scanning the parameter space until the observed probability distribution of the fluctuating order parameter matched the independently known universal fixed point form appropriate to the Ising universality class in the FSS limit [41].

### III. RESULTS

#### A. MSA results

In the following we present the MSA results for the two subtypes of phase diagram, denoted  $\alpha$  and  $\beta$ , that we have distinguished. For each subtype we discuss its form first in the space of the physical fields,  $(T, p, \Delta\mu)$ , and then in a mixed field-density space,  $(T, \rho, c)$ . Although representations in field space are somewhat less conventional than those in a mixed space of fields and densities, they do afford a compact display of results because two-phase coexistence occurs on surfaces. Taken together both representations provide a full picture of the characteristic features of the respective topologies. We note that as a consequence of the symmetry of the underlying model the field space representation is symmetric with respect to the plane  $\Delta\mu = 0$ , while the mixed space representation is symmetric with respect to  $c = 1/2$ .

##### 1. The type $\alpha$ phase diagram

Here we consider the phase behaviour of subtype  $\alpha$ . Motivated by the results of Pini *et al.* [19], we have obtained the phase behaviour using MSA for  $\delta = 0.67$ . We present first, in Fig. 1, the phase diagram in  $(T, p, \Delta\mu)$ -space. Four coexistence surfaces are distinguishable,  $\mathcal{R}_i^\alpha$ ,  $i = 1, \dots, 4$ , along each of which two phases coexist.  $\mathcal{R}_1^\alpha$  lies in the  $(\Delta\mu = 0)$ -plane and represents the demixing surface.  $\mathcal{R}_2^\alpha$  and  $\mathcal{R}_3^\alpha$  are symmetrically related and describe neither pure demixing transitions nor pure liquid-vapour (LV) transitions. Finally, along  $\mathcal{R}_4^\alpha$  there is (predominantly) LV coexistence. The lines of intersection between  $\mathcal{R}_2^\alpha$  and  $\mathcal{R}_3^\alpha$  with  $\mathcal{R}_4^\alpha$  are symmetrically related triple lines,  $\mathfrak{t}_2^\alpha$  and  $\mathfrak{t}_3^\alpha$ . On the high temperature side they terminate in critical end points (CEPs), which are connected by a critical line,  $\mathfrak{c}_4^\alpha$ , marking the upper edge of surface  $\mathcal{R}_4^\alpha$ . This critical line passes through the LV critical point of the field-free case, located at  $\Delta\mu = 0$ . The surfaces  $\mathcal{R}_2^\alpha$ ,  $\mathcal{R}_3^\alpha$ , and  $\mathcal{R}_4^\alpha$  thus form a pocket delimited by the critical line  $\mathfrak{c}_4^\alpha$  and the triple lines  $\mathfrak{t}_2^\alpha$  and  $\mathfrak{t}_3^\alpha$ . In this pocket a homogeneous, mixed fluid is stable as was observed previously in ref. [19]. Two further triple lines,  $\mathfrak{t}_1^\alpha$  and  $\mathfrak{t}_4^\alpha$ , can be found in the equimolar plane of  $\mathcal{R}_1^\alpha$ : they are the intersection lines of the two symmetrically related surfaces,  $\mathcal{R}_2^\alpha$  and  $\mathcal{R}_3^\alpha$ , with the demixing surface  $\mathcal{R}_1^\alpha$ . The fact that these three surfaces intersect in a line rather than in a point is a consequence of the symmetry of the system. All triple lines meet in the only quadruple point of the system. The equimolar triple line  $\mathfrak{t}_1^\alpha$  intersects at high temperatures the tricritical point of the system. At this point three critical lines,  $\mathfrak{c}_1^\alpha$ ,  $\mathfrak{c}_2^\alpha$ , and  $\mathfrak{c}_3^\alpha$ , originate: in the equimolar plane of  $\mathcal{R}_1^\alpha$  lies the critical line  $\mathfrak{c}_1^\alpha$  that characterizes the demixing transition (the so-called  $\lambda$ -line) and the two symmetrically related critical lines  $\mathfrak{c}_2^\alpha$  and  $\mathfrak{c}_3^\alpha$  that specify the mixing-demixing transition, and which tend (for  $|\Delta\mu| \rightarrow \infty$ ) towards the critical points of the respective pure components. If we focus on the isotherms that are marked in Fig. 1 we recover at a quantitative level the scenario depicted in Figs. 3(b) to (d) of ref. [19].

Turning next to the mixed field-density representation for subtype  $\alpha$  [i.e., in  $(T, \rho, c)$ -space], this is displayed in Fig. 2. Four distinct coexistence surfaces,  $\mathcal{S}_i^\alpha$ , are observable, corresponding to the respective  $\mathcal{R}_i^\alpha$ ,  $i = 1 \dots, 4$ . In this representation, however, the surfaces separate ‘two-phase’ regions (below) from regions of homogeneous phases (above). Again, surfaces intersect along triple lines now represented by three lines (branches). Each surface exhibits a critical line,  $\mathfrak{c}_i^\alpha$ .  $\mathcal{S}_1^\alpha$  is symmetrical with respect to the  $(c = 1/2)$ -plane and its critical line,  $\mathfrak{c}_1^\alpha$ , is the  $\lambda$ -line. On  $\mathcal{S}_1^\alpha$ , two symmetrical high-density phases ( $\rho \gtrsim 0.5$ ), specified by  $(\rho, c)$  and  $(\rho, 1-c)$ , are in coexistence. The two (symmetrically related) coexistence surfaces,  $\mathcal{S}_2^\alpha$  and  $\mathcal{S}_3^\alpha$ , are encountered for low and intermediate densities ( $\rho \lesssim 0.6$ ); the order parameter that characterizes this transition is a linear combination of the density and concentration differences of the two coexisting phases. Coming from high temperatures the  $\lambda$ -line bifurcates at the tricritical point into two critical lines,  $\mathfrak{c}_2^\alpha$  and  $\mathfrak{c}_3^\alpha$  (belonging to  $\mathcal{S}_2^\alpha$  and  $\mathcal{S}_3^\alpha$ ), which pass through minima (i.e., ‘double critical points’) and head for the respective LV critical points of the pure phases. The fourth coexistence surface,  $\mathcal{S}_4^\alpha$ , is predominantly LV-like in character and is located in between  $\mathcal{S}_2^\alpha$  and  $\mathcal{S}_3^\alpha$ . Its critical line passes through the LV critical point of the field-free mixture. The surface as a whole is delimited by the four intermediate-density branches of the triple lines  $\mathfrak{t}_2^\alpha$  and  $\mathfrak{t}_3^\alpha$  which form a lens-shaped ‘loop’. Tie-lines starting at these enclosing triple lines connect a vapour and a liquid phase of approximately equal concentrations with a liquid phase of higher density and different concentration [see  $(\rho, c)$ -projection of Fig. 2, where for each triple line a set of tie lines was selected]. The latter states form the high-density branch of the triple lines  $\mathfrak{t}_2^\alpha$  and  $\mathfrak{t}_3^\alpha$ , that are located in the ‘valley(s)’ formed by  $\mathcal{S}_2^\alpha$  (or  $\mathcal{S}_3^\alpha$ ) and  $\mathcal{S}_1^\alpha$ . In

$(T, \rho, c)$ -space the quadruple point can be localized as follows: its intermediate density representations are located on the end points of the lens-shaped ‘loop’, while the other two, being symmetrically related, are the bifurcation points of the triple lines  $\mathfrak{t}_2^\alpha$  and  $\mathfrak{t}_3^\alpha$ . As the critical line  $\mathfrak{c}_4^\alpha$  of  $\mathcal{S}_4^\alpha$  approaches the bounding triple lines  $\mathfrak{t}_2^\alpha$  and  $\mathfrak{t}_3^\alpha$ , the coexisting vapour and liquid phases become critical. Since these are simultaneously in equilibrium with a non-critical phase (the so-called spectator phase) located at the end point of the high-density branch of the triple lines, this point is a CEP. The region of a homogeneous, mixed fluid at intermediate densities found in [19] and discussed above in field space, is bounded by the three coexistence surfaces  $\mathcal{S}_2^\alpha$ ,  $\mathcal{S}_3^\alpha$ , and  $\mathcal{S}_4^\alpha$ .

We close with a more qualitative discussion of the type  $\alpha$  phase diagram which, nevertheless, might be rather instructive. In Fig. 3 we show the projection of the phase diagram in  $(T, \rho, c)$ -space onto the  $(T, \rho)$ -plane. In this representation we have introduced six temperature ranges (labeled A’ to F’); they are separated by five isotherms which are characterized by particular temperatures of the system. In Fig. 4 we show representative isothermal cuts taken from each of these temperature ranges in the  $(\rho, c)$ -plane. These figures complement those of Fig. 2 in ref. [19] in the sense that they present a more comprehensive sequence of possible scenarios of coexistence regions encountered in the type  $\alpha$  phase diagram. However, we note that within subtype  $\alpha$ , other scenarios in the isothermal cuts can also be observed. This is, for instance, the case when the LV critical point lies *above* the temperature that characterizes the minimum in the symmetrically related critical lines  $\mathfrak{c}_2^\alpha$  and  $\mathfrak{c}_3^\alpha$  that pass through the equimolar tricritical point. Hence, scenarios different to the ones presented here can be encountered. In range A’, i.e., at temperatures below the quadruple point, regions of homogeneous phases are only found at low densities (extending over all concentrations), and in small areas at high densities (with concentrations close to 0 or 1). As indicated by the tie lines, two-phase coexistence is generally observed; only at  $c = 1/2$  and low densities and at the symmetrically related corners of the homogeneous high density phases does three phase coexistence occur. At the temperature of the quadruple point, an infinitesimal amount of a fourth homogeneous phase emerges at  $c = 1/2$  and  $\rho \simeq 0.45$ . As we proceed to range B’, this point extends to a small region where a homogeneous phase exists (see the discussion above); as can be seen from the tie lines, its three corners are points of three phase coexistence. Furthermore the other regions of homogeneous phases encountered already in range A’ grow both in density and concentration.

By further increasing the temperature we pass through the equimolar LV critical point and reach range C’. Now a narrow passage has opened up between the homogeneous mixed fluid ( $c \sim 1/2$  and  $\rho \sim 0.5$ ) and the homogeneous low density phases, that becomes broader with increasing temperature. It is characterized by two critical points located on the symmetrically related coexistence regions. At some temperature these become CEPs and we enter the range D’. Here the scenario is dominated by three huge, interconnected coexistence regions: one is symmetrical with respect to  $c = 1/2$  at high density and two are symmetrically related (one for  $c \gtrsim 0.6$ , the other one for  $c \lesssim 0.4$ ). In the range D’, the coexistence regions are nearly entirely two-phase in character; three-phase coexistence is only observed at intermediate and high densities. The next transition temperature is characterized by the minimum of the symmetrically related critical lines  $\mathfrak{c}_2^\alpha$  and  $\mathfrak{c}_3^\alpha$  that originate at the tricritical point and head towards the critical points of the pure components. As we pass this temperature, we enter range E’ and the connections between the three coexistence regions break, leaving them entirely disconnected. Four critical points can now be observed: two of them are located on the symmetrically related coexistence regions and two others (symmetrically related), can be found on the demixing coexistence region. In small areas, close to these regions, three-phase coexistence is observed. As we finally pass through the tricritical point of the system we enter range F’, where the three coexistence regions are well-separated and the phase diagram is dominated by huge areas of homogeneous mixtures. The coexistence regions now show exclusively two-phase coexistence. The two critical points of the demixing coexistence region have merged at the tricritical point to a single critical point (located on the  $\lambda$ -line).

## 2. The type $\beta$ phase diagram

In the type  $\beta$  phase diagram, which we have found to occur at  $\delta = 0.69$ , the phase behaviour is distinct from that of type  $\alpha$ . In the  $(T, p, \Delta\mu)$ -space representation of Fig. 5 we can again clearly identify four coexistence surfaces  $\mathcal{R}_i^\beta$ ,  $i = 1, \dots, 4$ . However, the manner of their intersection engenders a different topology. The triple line  $\mathfrak{t}_4^\beta$  is now the intersection of the surfaces  $\mathcal{R}_1^\beta$  and  $\mathcal{R}_4^\beta$ . Intersection of  $\mathcal{R}_2^\beta$  and  $\mathcal{R}_3^\beta$  with  $\mathcal{R}_1^\beta$  leads again to the triple line  $\mathfrak{t}_1^\beta$ , in the  $(\Delta\mu = 0)$ -plane, which terminates at high temperatures at the tricritical point. From there, (and similarly to type  $\alpha$ ), three critical lines originate: the  $\lambda$ -line (i.e., the critical line  $\mathfrak{c}_1^\beta$  of  $\mathcal{R}_1^\beta$ ) continues to higher temperatures, while two symmetrically related critical lines,  $\mathfrak{c}_2^\beta$  and  $\mathfrak{c}_3^\beta$ , head off to lower temperatures. These terminate in two CEPs where they also meet two symmetrically related triple lines,  $\mathfrak{t}_2^\beta$  and  $\mathfrak{t}_3^\beta$ . Along these lines  $\mathcal{R}_2^\beta$  and  $\mathcal{R}_3^\beta$  intersect with  $\mathcal{R}_4^\beta$  (which is a predominantly LV coexistence surface) and which dominates the low pressure region and covers the whole  $\Delta\mu$ -range. The intersection of  $\mathfrak{t}_2^\beta$  and  $\mathfrak{t}_3^\beta$  with the aforementioned triple lines  $\mathfrak{t}_1^\beta$  and  $\mathfrak{t}_4^\beta$ , in the  $(\Delta\mu = 0)$ -plane,

gives rise to the only quadruple point of the system.  $\mathcal{R}_4^\beta$  is delimited at high temperatures by a further critical line,  $\mathbf{c}_4^\beta$ , which connects the critical points of the pure components (i.e., for  $|\Delta\mu| \rightarrow \infty$ ) with the LV critical point of the mixture at  $\Delta\mu = 0$ .

Again considering the mixed field-density representation in  $(T, \rho, c)$ -space, the distinction between type  $\beta$  and type  $\alpha$  phase diagrams is clear. The type  $\beta$  case is depicted in Fig. 6. Four coexistence surfaces  $\mathcal{S}_i^\beta$  with accompanying critical lines  $\mathbf{c}_i^\beta$  can be identified; they correspond to the respective  $\mathcal{R}_i^\beta$ . The  $\lambda$ -line ( $\mathbf{c}_1^\beta$ ), being the critical line of the symmetrical demixing surface  $\mathcal{S}_1^\beta$ , bifurcates at the tricritical point into two critical lines,  $\mathbf{c}_2^\beta$  and  $\mathbf{c}_3^\beta$ , which traverse the (symmetrically related) surfaces  $\mathcal{S}_2^\beta$  and  $\mathcal{S}_3^\beta$ . Passing through minima (i.e., ‘double critical points’) these critical lines terminate in CEPs located at the symmetrically related high density branches of the triple lines,  $\mathbf{t}_2^\beta$  and  $\mathbf{t}_3^\beta$ . These triple lines are the intersection of  $\mathcal{S}_2^\beta$  and  $\mathcal{S}_3^\beta$  with coexistence surface  $\mathcal{S}_4^\beta$  that encompasses the entire concentration range. At these CEPs, two high-density phases become critical while in coexistence with the spectator phase located at the end points of the low-density branches of the triple lines. The critical line  $\mathbf{c}_4^\beta$  on  $\mathcal{S}_4^\beta$  passes through the equimolar LV critical point and connects the critical points of the respective pure components; in contrast to type  $\alpha$  it is now completely detached from the  $\lambda$ -line. In subtype  $\beta$  the triple lines also show a distinctively different behaviour than their equivalents in subtype  $\alpha$ . As can be seen from the representative tie lines (all connecting coexistence points on triple lines) shown in Fig. 6, a single low-density phase (with  $c \simeq 1/2$ ) is connected via tie lines to two high-density phases. In contrast to type  $\alpha$ , the high and the intermediate density triple lines,  $\mathbf{t}_1^\beta$ ,  $\mathbf{t}_2^\beta$ , and  $\mathbf{t}_3^\beta$ , merge to form two symmetrically related ‘loops’, while the low density branches terminate as the spectator phase of the CEPs. Again, for  $\rho \sim 0.5$  a region of a homogeneous, mixed fluid is encountered, which is enclosed by the coexistence surfaces  $\mathcal{S}_2^\beta$ ,  $\mathcal{S}_3^\beta$ , and  $\mathcal{S}_4^\beta$  (see also ref. [19]). At the quadruple point, the low density branch of  $\mathbf{t}_4^\beta$  bifurcates in the low density branches of  $\mathbf{t}_2^\beta$  and  $\mathbf{t}_3^\beta$ , whereas the high density branches of  $\mathbf{t}_4^\beta$  bifurcate in the high density branches of  $\mathbf{t}_2^\beta$  (and symmetrically related  $\mathbf{t}_3^\beta$ ) and  $\mathbf{t}_1^\beta$ . The fourth representation of the quadruple point is located in the ‘valley’ of mixed fluid, where the intermediate branches of  $\mathbf{t}_2^\beta$ ,  $\mathbf{t}_3^\beta$ , and  $\mathbf{t}_1^\beta$  intersect.

Again we close the discussion of the type  $\beta$  phase diagram with a more qualitative discussion. In Fig. 7 we show projections of characteristic lines of the phase diagram onto the  $(T, \rho)$ -plane, defining six temperature ranges, labeled A to F. In Fig. 8 we show isothermal cuts for each of these temperature ranges. In the type  $\beta$  phase diagram the scenarios in the temperature ranges A and B (which are again separated by the quadruple point temperature) correspond on a qualitative level exactly to the corresponding ones in type  $\alpha$ . In particular, in range B we again encounter three large interconnected coexistence regions with a small area of a homogeneous, mixed fluid for  $c \sim 1/2$  and  $\rho \sim 0.5$ . The minimum on the symmetrically related critical lines,  $\mathbf{c}_2^\beta$  and  $\mathbf{c}_3^\beta$ , on  $\mathcal{S}_2^\beta$  and  $\mathcal{S}_3^\beta$  (mentioned above) define the temperature where we enter range C: in contrast to type  $\alpha$ , the three large coexistence regions break up at  $\rho \gtrsim 0.5$ , splitting off the demixing coexistence region and leaving the other two connected. The symmetrically related passages are characterized by pairs of critical points (located on each of the two coexistence regions in a 3d representation in  $(T, \rho, c)$ -space), and connected by symmetrically related critical lines  $\mathbf{c}_2^\beta$  and  $\mathbf{c}_3^\beta$  that originate in the tricritical point and terminate at symmetrically related CEPs. This CEP-temperature marks the limit between ranges C and D. In range D only the symmetrically related critical points on the demixing surface remain; simultaneously, the connecting bridge between the large coexistence regions that extend over all concentrations becomes narrower. Passing the equimolar LV critical point (and thus entering range E) this connection breaks up leading to two symmetrically related coexistence regions that are entirely detached from the demixing region, and on each of which a pair of symmetrically related critical points emerges. Finally, above the tricritical point of the system (i.e., in the range F) the three coexistence regions are by now well separated, each being characterized by a critical point, which corresponds exactly to the scenario depicted for the range F’ in subtype  $\alpha$ . Again we note that within subtype  $\beta$ , slightly different scenarios in the isothermal cuts can be observed. This is, for instance, the case if the equimolar LV critical temperature is lower than the temperature of the minimum in the symmetrically related triple lines,  $\mathbf{t}_2^\beta$  and  $\mathbf{t}_3^\beta$ .

### 3. The transition scenario

Of course it is of particular interest how the transition from one subtype to the other takes place. We start from subtype  $\alpha$  and increase the parameter  $\delta$ . In the  $(T, p, \Delta\mu)$ -representation the transition scenario between the two subtypes can be traced easily. The characteristic pocket formed by  $\mathcal{R}_2^\alpha$ ,  $\mathcal{R}_3^\alpha$ , and  $\mathcal{R}_4^\alpha$  becomes larger by extending the limiting triple line branches,  $\mathbf{t}_2^\alpha$  and  $\mathbf{t}_3^\alpha$  (and thus the connecting critical line  $\mathbf{c}_4^\alpha$ ) in both directions. Simultaneously the symmetrically related critical lines  $\mathbf{c}_2^\alpha$  and  $\mathbf{c}_3^\alpha$  that emerge from the tricritical point are shifted to lower temperatures. At the transition value  $\tilde{\delta}$ , these critical lines have reached the CEPs, thereby forming two additional, symmetrically related tricritical points. As a consequence the coexistence surface  $\mathcal{R}_2^\alpha$  is subdivided by the triple line  $\mathbf{t}_2^{\text{tr}}$  (the former

$t_2^\alpha$ ), into two sub-surfaces,  $\mathcal{R}_{2'}^{\text{tr}}$  and  $\mathcal{R}_{2''}^{\text{tr}}$ . The same happens with the symmetrically related surface  $\mathcal{R}_3^\alpha$ . A three sided pocket is now formed by  $\mathcal{R}_{2'}^{\text{tr}}$ ,  $\mathcal{R}_{3'}^{\text{tr}}$ , and  $\mathcal{R}_4^{\text{tr}}$  (the former  $\mathcal{R}_4^\alpha$ ). From below it is bounded by the quadruple point, its edges are the triple lines, the upper three corners are the tricritical points which, in turn, are connected by sections of the critical lines (see below). Upon further increasing  $\delta$ ,  $\mathcal{R}_4^{\text{tr}}$  merges with  $\mathcal{R}_{2'}^{\text{tr}}$  and  $\mathcal{R}_{3'}^{\text{tr}}$  forming thus  $\mathcal{R}_4^\beta$  while  $\mathcal{R}_{2''}^{\text{tr}}$  ( $\mathcal{R}_{3''}^{\text{tr}}$ ) becomes  $\mathcal{R}_2^\beta$  ( $\mathcal{R}_3^\beta$ ). The surface  $\mathcal{R}_1^\alpha$  is not affected by the transition and corresponds to  $\mathcal{R}_1^\beta$ . In a similar manner the critical line  $c_2^\alpha$  (and symmetrically related  $c_3^\alpha$ ) is subdivided at the transition in two sections  $c_{2'}^{\text{tr}}$  and  $c_{2''}^{\text{tr}}$ , where  $c_{2'}^{\text{tr}}$  is delimited by the field-free tricritical point and one of the newly formed tricritical points.  $c_4^{\text{tr}}$  is limited by the newly formed tricritical points. Upon further increasing  $\delta$ ,  $c_4^{\text{tr}}$ ,  $c_{2''}^{\text{tr}}$ , and  $c_{3''}^{\text{tr}}$  merge to form  $c_4^\beta$ .  $c_{2'}^{\text{tr}}$  ( $c_{3'}^{\text{tr}}$ ) becomes  $c_2^\beta$  ( $c_3^\beta$ ) and are delimited by CEPs and the field-free tricritical point.

To discuss the transition scenario in the  $(T, \rho, c)$ -representation we again start from type  $\alpha$  and increase  $\delta$ . Then gradually the high- and the intermediate-density branches of the triple lines  $t_2^\alpha$  and  $t_3^\alpha$  lengthen until they merge when the CEP located on the intermediate-density branch meets the end point of the high-density branch, thereby forming a tricritical point (see Fig. 9). Upon further increase of  $\delta$ , a high-density branch (with a CEP) and a low-density branch of the triple line detach, thus resulting in the topology of the  $\beta$ -subtype. Concomitant with this metamorphosis of the triple lines, we observe a related development in the critical line  $c_4^\alpha$  that passes through the LV critical point in subtype  $\alpha$ : with increasing  $\delta$ , this line lengthens in both directions until it meets (at the crossover between the subtypes) the critical lines of the surfaces  $\mathcal{S}_2^\alpha$  and  $\mathcal{S}_3^\alpha$ . As  $\delta$  is further increased, a new critical line forms connecting the critical points of the pure phases, passing through the equimolar LV critical point so that the CEPs remain with the newly formed triple lines at higher densities.

Within the MSA the transition occurs for  $\tilde{\delta}_{\text{MSA}} = 0.678(0)$ . We derive this estimate by following the development of the triple lines  $t_2^\alpha$  and  $t_3^\alpha$  to  $t_2^\beta$  and  $t_3^\beta$  with increasing  $\delta$ . In both subtypes, two of the three branches of the triple lines mentioned above meet each other in CEPs, whereas at the transition all three branches meet in a tricritical point. Fig. 9 shows a selection of the triple lines  $t_3^\alpha$  and  $t_3^\beta$  for different values of  $\delta$ .

The transition scenario (although not explicitly identified there) is nicely depicted on several occasions in [19]. Within the MF framework, where the transition occurs at  $\tilde{\delta}_{\text{MF}} = 0.65338$ , the above mentioned loop of critical lines is nicely depicted in Fig. 1(c). Figs. 10 and 12 show projections of the HRT  $(T, \rho, c)$  phase diagram onto the  $(\rho, c)$ -plane at various temperatures for  $\delta = 0.67$ , while in Fig. 11 isothermal cuts through the  $(T, p, \Delta\mu)$  phase diagram are shown. This  $\delta$ -value is close to the HRT-transition value,  $\tilde{\delta}_{\text{HRT}}$ .

#### 4. Relationship to previous theoretical work

The two subtypes that we discuss here have already been classified by van Konynenburg and Scott [1]: type  $\alpha$  corresponds to ‘sym. III-A\*’ while type  $\beta$  to type ‘sym. II-A\*’. Several years later Antonevych *et al.* [14] pointed out that the complex topology of the *full* phase diagram of a binary symmetrical mixture originates from the complex interplay of the LV transition and the demixing transition (see Figs. 1 to 4 in this contribution). However, most of their considerations were carried out on a *qualitative* level (see section III.B of ref. [14]).

Shortly afterwards, Pini *et al.* [19] presented their remarkable HRT and MF theoretical study of the full phase diagram of binary symmetrical mixtures, discovering several interesting features which they presented in the form of isothermal cuts through the phase diagrams in  $(T, p, \Delta\mu)$ - and in  $(T, \rho, c)$ -space. The two subtypes that we have discussed here in detailed were identified in their contribution as the two alternative ways in which the region of the homogeneous fluid occurring at intermediate densities (see above) is formed from the intersection of the coexistence surfaces. Additionally, the authors pointed out that in what we term subtype  $\alpha$ , the critical temperature at  $\Delta\mu = 0$  is always lower than the tricritical temperature, while in subtype  $\beta$  no such ordering relation holds. While Pini *et al.* focus in their contribution on a classification of the topology via the critical lines, we consider a discussion of the phase diagrams via the location of the triple lines to be more enlightening. In fact, our 3d representations both in the space of the physical fields as well as in the mixed field-density space helped us to clarify the following points: (i) from these representations we obtained an unambiguous identification of two distinct subtypes (confirming also the conclusions drawn in [19]); (ii) in the 3d plots, the ‘double critical points’ reported in [19] are identifiable as local minima in the critical lines; (iii) we find previously unreported triple lines; (iv) the transition scenario between the two subtypes could be discussed and clarified in detail (see sec. III A 3). Comparison of our isothermal cuts with those presented by Pini *et al.* facilitates the link between our subtypes and the topological changes identified in [19]: in their Figs. 2, 3, 6, and 7 a type  $\alpha$  behaviour can be identified, while Figs. 8 and 9 display a  $\beta$  topology; Figs. 10 to 12 depict a close-to-transition scenario (see also sec. III A 3).

Finally, Woywod and Schoen [24] have very recently studied a lattice model using a MF density functional theory, to calculate the complete phase diagram of a binary fluid mixture of equally sized particles. The conclusions that the authors could draw from their investigations are relevant also for the present study: they present arguments (that back



up earlier conclusions [42]) which preclude the existence of tricritical points in *general* binary mixtures, but allow them under certain symmetry conditions which are fulfilled by symmetrical mixtures, but can also be found in particular asymmetric mixtures such as those investigated in [24]. Their investigations of the binary *symmetrical* mixture is focused on the shape of the phase diagram in field space for selected values of a parameter  $\Lambda$ , that characterizes the relative strength of the mixed interaction (cf. [1]), thus following essentially the sequence of systems summarized in Table I. However, the existence of the two subtypes  $\alpha$  and  $\beta$  is not mentioned at all in this contribution. However, due to the fact that Woywod and Schoen could calculate thermodynamic potentials via an essentially closed expression, they were able to pin down exactly the transition scenario discussed in sec. III A 3. In particular in their Fig. 5 this transition in the  $(T, \mu, \Delta\mu)$ -space is clearly depicted, showing explicitly the three tricritical points, the quadruple point, and the connecting critical and triple lines that occur for this particular system. We point out that for the semi-analytical approach used in the present contribution within the MSA framework, such an exact localization of the transition is beyond reach.

## B. Simulation results

Turning now to the results of our GCMC simulations, our strategy for mapping the coexistence behaviour was initiated on the symmetry plane  $\Delta\mu = 0$ , where we first mapped the phase diagram in the  $(\mu_1, T)$ -plane. Use of histogram reweighting then provided estimates for the phase behaviour at small, but finite,  $\Delta\mu$ . Guided by this prediction, a new set of simulations were subsequently performed at near coexistence state points for this value of  $\Delta\mu$ , the results of which were extrapolated to yet larger  $\Delta\mu$ , and so on. In this manner we were able to track the phase behaviour as a function of  $\Delta\mu$  and cover a large range of concentrations in the process. By accumulating separately contributions to the energy from like and unlike particle interactions, we were further able to perform histogram extrapolation with respect to  $\delta$ . This was useful in helping to find the regions of  $\delta$  relevant to the two subtypes.

The high dimensionality of the full phase diagram precludes a comprehensive study of the full 3d phase diagram as was done via MSA. Nevertheless projections of our data onto the  $(T, \rho)$ -,  $(\rho, c)$ -, and  $(T, c)$ -planes, as shown in Figs. 10 and Figs. 12, clearly confirm the existence of the two subtypes seen in the corresponding projections of the MSA data (Fig. 2 and 6) and detailed above, albeit at slightly different values of  $\delta$ . Specifically, for  $\delta = 0.66$ , the critical lines emanating from the tricritical point links up with that coming from the LV critical points of the pure phases, while the critical line emanating from the field-free LV critical point terminates at two symmetrically related CEPs at which a demixed high density non-critical (spectator) phase coexists with a lower density critical phase. The phase that coexist at the CEPs are joined in Figs. 10(a)-(c) via a dashed line. The character of the CEP behaviour is clarified by the measured forms of the density and concentration distributions, as shown in Fig. 11. The form of  $P(\rho)$  for the critical phase has a highly non-Gaussian structure which matches the universal Ising order parameter distribution appropriate for a critical finite-sized system (see inset) [11, 16, 32]. That the critical phase is predominantly liquid-vapor in character is evidenced by the absence of strong concentrations fluctuations as reflected in the near-Gaussian form of  $P(c)$  for the lower density phase.

For  $\delta = 0.68$ , the results of Figs. 12 shows that the phase behaviour is of subtype  $\beta$ . Specifically, the LV critical point of the pure phases joins smoothly to that of the equimolar mixture, while the critical line emanating from the tricritical point terminate at two symmetrically related CEPs, the coexisting phase of which are joined by dashed lines in Figs. 12. The nature of these CEPs is again elucidated by the corresponding forms of  $P(\rho)$  and  $P(c)$  (see Fig. 13). One finds now that the spectator phase is a low density mixed phase, while the higher density critical phase exhibits fluctuations that are neither predominantly density-like nor concentration-like in character, but a coupled mixture of the two. Thus the forms of  $P(\rho)$  and  $P(c)$  for the critical phase both exhibit forms that are highly non-Gaussian in nature, though neither matches well the universal Ising form. In such situations one can expect that the true order parameter for this transition involves a linear combination of density, concentration (and energy), though we have not attempted to investigate this matter further here.

As regards the range of  $\delta$  in which the two subtypes of phase behaviour occur, the simulation results are in semi-quantitative agreement with the MSA calculations. However, owing to the computational burden of this problem, we were not able to pin down precisely the value of  $\tilde{\delta}$  at which the transition between subtypes occurs, although our results shows that  $\tilde{\delta}$  differs from that found in MSA by at most 0.01.

## IV. DISCUSSION AND CONCLUSIONS

To summarize, we have investigated the full phase behaviour of a symmetrical binary fluid in a range of model parameters for which, at equal chemical potentials, the system exhibits a LV critical point and a tricritical point. The

phase behaviour is considerably richer in both variety and character than would be expected on the basis of knowledge of the field-free case alone. Our results confirm previous less detailed reports that for unequal chemical potentials, two subtypes  $\alpha$  and  $\beta$  of phase behaviour occur, and we have elucidated the differences between these subtypes in terms of the topologies of triple lines and critical lines.

The MSA results are in semi-quantitative agreement with those of MC simulations, demonstrating that MSA provides a correct description of this system. Use of the MSA should therefore prove useful in narrowing down simulating searches of parameter space when seeking a given type of phase behaviour. Moreover, our study has demonstrated that simulations are competitive with theory in providing (within a reasonable amount of time) precise information on intricate phase diagrams exhibiting complex topologies of critical lines. Given that the various commonly used theoretical approaches (HRT, SCOZA, MSA, ...) do not always agree, MC thus provides an invaluable benchmark with which to compare. We note that our results are in good agreement with the less comprehensive MF and HRT study of these two subtypes in ref. [19]. Although HRT is generally more accurate than MSA, it is very laborious to implement and computationally expensive, and still does not produce results in fully quantitative agreement with simulation, as has been observed in studies of the field-free case [16].

As regards the more general relevance of our findings, one can consider the symmetrical binary fluid model as probably the simplest member of a class of one component ‘spin’-fluid models in which the particles carry an orientational degree of freedom which features in their interparticle potentials [13, 19]. Other, more complex examples include Heisenberg [43], Ising [44], or dipolar spin fluids [45]. It is well known that similar sequences of phase diagram topologies can arise in all members of this class and that one-to-one correspondences can generally be made between the phases of the binary symmetrical mixture and those exhibited by the more complex models. However studies of phase behaviour for the more complex class members have to be performed using more complicated techniques than the MSA. Thus the symmetrical mixture plays a key (computationally tractable) role in elucidating generic aspects of the phase behaviour.

As regards future work, it would be of interest to extend the present studies to encompass the more general case of asymmetrical mixtures. Steps in this direction, have recently been reported for the case of a lattice based binary fluid model [24], though this is unable to represent particle species of unequal sizes, whose packing effects are likely to be subtle. From the simulation point of view, GCMC simulations of asymmetrical mixtures are not significantly more challenging than the symmetrical case, provided the size asymmetry is moderate. Recent methods for minimizing finite-size effects in GCMC measurements of coexistence properties of fluid mixtures, should also help render this a practical proposition [47].

## APPENDIX: NUMERICAL SOLUTION OF THE MSA

We were able to perform all our MSA calculations using `MATHEMATICA`<sup>TM</sup> [30] in a rather straightforward fashion. Phase diagrams of *general* (i.e., non-symmetrical) binary mixture are also accessible via this numerical route.

We start with the determination of the phase diagram in  $(T, \rho, c)$ -space. To determine at a given temperature  $T$ , the concentrations and densities of two coexisting phases (labeled I and II) one solves the following (coexistence) equations numerically, e.g. with a Newton-Raphson algorithm

$$\Delta\mu_1^{(\text{I-II})}(\mathbf{z}) = 0 \tag{A.1}$$

$$\Delta\mu_2^{(\text{I-II})}(\mathbf{z}) = 0 \tag{A.2}$$

$$\Delta p^{(\text{I-II})}(\mathbf{z}) = 0, \tag{A.3}$$

here  $\mathbf{z} = \{c_{\text{I}}, c_{\text{II}}, \rho_{\text{I}}, \rho_{\text{II}}; T\}$ . The  $\Delta\mu_i^{(\text{I-II})}$ ,  $i = 1, 2$ , are the differences between the chemical potentials of the respective species of the coexisting phases and  $\Delta p^{(\text{I-II})}$  is the difference between the corresponding pressures.

At fixed  $T$ , equations (A.1) to (A.3) represent three relations between four unknown quantities, i.e.,  $c_{\text{I}}, c_{\text{II}}, \rho_{\text{I}}$ , and  $\rho_{\text{II}}$ . To solve this set of nonlinear equations one requires an additional constraint, which can contain any subset of the unknown quantities. The proper choice of such a constraint is important since it has a distinct influence on the efficiency of the calculation of coexistence curves. The simplest (and most obvious) restriction is to fix the value of a particular variable and use it to parameterize the coexistence curve. For example, if we wish to calculate, at a given  $T$ , a LV coexistence line, we may fix the value of the concentration of the vapour phase,  $c_{\text{I}}$ , and solve equations (A.1) to (A.3) for  $c_{\text{II}}, \rho_{\text{I}}$ , and  $\rho_{\text{II}}$ . In order to proceed to a neighboring pair of coexisting states, we then add to this solution,  $\mathbf{z}$  say, a set of parameters  $\Delta\mathbf{z} = \{\Delta c, 0, 0, 0\}$ , i.e.,  $\mathbf{z}' = \mathbf{z} + \Delta\mathbf{z}$ , which constitutes a starting point for solving the coexistence equations for the new pair of coexisting states. The step size  $\Delta c$  in the concentration  $c_{\text{I}}$  depends on the form of the coexistence lines. Solution of the coexistence equations leads to a neighboring pair of coexisting states.

Given any two states, new initial values for coexistence points can be obtained via linear extrapolation from the previous states, thus facilitating use of a larger step-size in  $\Delta c$ .

For a triple line (i.e., for three-point coexistence) we have to satisfy, in addition to equations (A.1) to (A.3), the relations

$$\Delta\mu_1^{(\text{II-III})}(\mathbf{z}) = 0 \quad (\text{A.4})$$

$$\Delta\mu_2^{(\text{II-III})}(\mathbf{z}) = 0$$

$$\Delta p^{(\text{II-III})}(\mathbf{z}) = 0$$

(A.5)

with  $\mathbf{z}$  being now  $\mathbf{z} = \{c_{\text{I}}, c_{\text{II}}, c_{\text{III}}, \rho_{\text{I}}, \rho_{\text{II}}, \rho_{\text{III}}; T\}$ . For fixed temperature  $T$  we thus have six equations for six unknowns, i.e., no additional constraint is required.

The above considerations provide a recipe for locating coexisting states, once a solution is known. An appropriate starting point for the iteration outlined above is a coexistence point of the pure fluids, i.e., for  $c = 0$  or  $c = 1$ , for which either equation (A.1) or (A.2) is trivially satisfied. Starting at a rather low temperature coexisting state of the pure fluid, we employ the above stepwise approach to calculate a *full* isothermal cut. While for these temperatures the coexistence lines of the vapour phase reach the symmetric plane at  $c = 1/2$ , this is not the case for the coexistence line of the fluid phase: they terminate instead at the high-density branch of the symmetrically related triple lines  $t_2$  and  $t_3$ . By gradually increasing the temperature we can trace this pair of triple lines to higher temperatures and use them at the same time to determine the isothermal cuts of the demixing coexistence surface,  $\mathcal{S}_1$ . For this region of the phase diagram, we again take advantage of the symmetry of the system. The variable  $\mathbf{z}$  is then given by  $\mathbf{z} = \{c_{\text{II}}, c_{\text{III}} (= 1 - c_{\text{II}}), \rho_{\text{II}}, \rho_{\text{III}} (= \rho_{\text{II}})\}$ . In this case equations (A.1) and (A.2) are identical and relation (A.3) is trivially fulfilled for equal densities. Using coexisting states at a given density and temperature as starting points, we scan the demixing surface by gradually increasing the temperature at fixed density.

Particular care has to be paid to the determination of the critical points which, as a function of temperature, form the critical lines. Since MSA can become numerically unstable in the vicinity of a critical point, we have sought to localize critical lines within narrow intervals. To this end we have calculated coexistence states characterized by a fixed, narrow ‘distance’  $d$ , with  $d^2 = (c_{\text{I}} - c_{\text{II}})^2 + (\rho_{\text{I}} - \rho_{\text{II}})^2$ ; for  $d$  we have assumed a value of 0.04. In this manner a good estimate for the critical line is obtained from the mean value of the concentrations and densities of the coexisting phases that fulfill the constraint.

The procedure outlined above permits construction of the four coexistence surfaces,  $\mathcal{S}_i^\gamma$  ( $\gamma = \alpha$  or  $\beta$  and  $i = 1, \dots, 4$ ). The final shape of the phase diagram is then obtained from the intersections of these coexistence surfaces; this leads – as we have learned from the discussion above – to the triple lines. These triple lines, which are a key feature of the phase diagram, constitute the boundaries of the coexistence surfaces, and truncate metastable regions of the coexisting surfaces, thus defining the final shape of the *full* phase diagram.

Once the phase diagram is determined in  $(T, \rho, c)$ -space, we calculate for coexisting states the corresponding thermodynamic properties (notably the pressure and the chemical potential) and determine with these quantities the phase diagram in  $(T, p, \Delta\mu)$ -space.

## ACKNOWLEDGMENTS

JK and GK acknowledge financial support by the Österreichische Forschungsfond (FWF) under Project Nos. P15758-N08, P17823-N08 and P17178-N02, the Hochschuljubiläumsstiftung der Stadt Wien under Project No. 1080/2002, and the Außeninstitut der TU Wien. Additional financial support was provided by the Anglo-Austrian ARC Programme of the British Council. The authors would like to thank Elisabeth Schöll-Paschinger (Wien) and Davide Pini (Milan) for useful discussions.

- 
- [1] P.H. van Konynenburg and R.L. Scott, *Philos. Trans. R. Soc. London, Ser. A* **51**, 495 (1980).
- [2] J.S. Rowlinson and F.L. Swinton, *Liquids and Liquid Mixtures*, Butterworth (London, 1982), 3rd edition.
- [3] J.-P. Hansen and I.R. McDonald, *Theory of Simple Liquids* (Cambridge, 2006), 3rd edition.
- [4] D. Frenkel and B. Smit, *Understanding Molecular Simulation*, (Academic Press, London, 2002), 2nd edition.
- [5] D.P. Landau and K. Binder, *A guide to Monte Carlo simulations in statistical physics*, Cambridge 2000.
- [6] A.Z. Panagiotopoulos, N. Quirke, M. Stapleton, and D.J. Tildesley, *Mol. Phys.* **63**, 527 (1988).
- [7] R.J. Recht and A.Z. Panagiotopoulos, *Mol. Phys.* **80**, 843 (1993).
- [8] C. Caccamo and G. Giunta, *Mol. Phys.* **78**, 83 (1993).
- [9] D.G. Green, G. Jackson, E. de Miguel, and L.F. Rull, *J. Chem. Phys.* **101**, 3190 (1994).
- [10] E. de Miguel, E.M. del Río, and M.M. Telo da Gama, *J. Chem. Phys.* **103**, 6188 (1995).
- [11] N.B. Wilding, *Phys. Rev. E* **55**, 6624 (1997); N.B. Wilding *Phys. Rev. Lett.* **78**, 1488 (1997).
- [12] C. Caccamo, D. Costa, and G. Pellicane, *J. Chem. Phys.* **109**, 4498 (1998).
- [13] N.B. Wilding, F. Schmid, and P. Nielaba, *Phys. Rev. E* **58**, 2201 (1998).
- [14] O. Antonevych, F. Forstmann, and E. Diaz-Herrera, *Phys. Rev. E* **65**, 061504 (2002).
- [15] G. Kahl, E. Schöll-Paschinger, and A. Lang, *Chemical Monthly* **132**, 1413 (2001).
- [16] N.B. Wilding, *Phys. Rev. E* **67**, 052503-1 (2003).
- [17] D. Woywod and M. Schoen, *Phys. Rev. E* **67**, 026122 (2003).
- [18] E. Schöll-Paschinger and G. Kahl, *J. Chem. Phys.* **118**, 7414 (2003).
- [19] D. Pini, M. Tau, A. Parola, and L. Reatto, *Phys. Rev. E* **67**, 046116-1 (2003).
- [20] E. Schöll-Paschinger, E. Gutleiderer, and G. Kahl, *J. Molec. Liquids* **112**, 5 (2004).
- [21] E. Schöll-Paschinger, D. Levesque, J.-J. Weis, and G. Kahl, *J. Chem. Phys.* **122**, 024507-1 (2005).
- [22] E. Schöll-Paschinger and G. Kahl, *J. Chem. Phys.* **123**, 134508-1 (2005).
- [23] E. Paschinger, D. Levesque, G. Kahl, and J.-J. Weis, *Europhys. Lett.* **55**, 178 (2001); E. Schöll-Paschinger, D. Levesque, J.-J. Weis, and G. Kahl, *Phys. Rev. E* **64**, 011502 (2001).
- [24] D. Woywod and M. Schoen, *Phys. Rev. E* **73**, 011201 (2006).
- [25] A. Parola and L. Reatto, *Adv. Phys.* **44**, 211 (1995); A. Parola and L. Reatto, *Phys. Rev. A* **44**, 6600 (1991); for a more recent overview see also: [19] and [26].
- [26] A. Reiner and G. Kahl, *Phys. Rev. E* **65**, 046701-1 (2002); A. Reiner and G. Kahl, *J. Chem. Phys.* **117**, 4925 (2002).
- [27] A brief summary of some aspects of this work has previously appeared elsewhere: J. Köfinger, G. Kahl, and N.B. Wilding, *Europhys. Lett.* **75**, 234 (2006).
- [28] L. Blum and J.S. Høye, *J. Stat. Phys.* **19**, 317 (1978).
- [29] E. Arrieta, C. Jędrzejek, and K. N. Marsh, *J. Chem. Phys.* **86**, 3607 (1987); *ibid.* **95**, 6806 (1991).
- [30] *Wolfram Research Inc.*, <http://www.wolfram.com>.
- [31] D. Pini, G. Stell, and R. Dickman, *Phys. Rev. E* **57**, 2862 (1998); D. Pini, G. Stell, and N.B. Wilding, *Mol. Phys.* **95**, 483 (1998).
- [32] N.B. Wilding, *Phys. Rev. E*, **52**, 602 (1995).
- [33] R.L. Scott, *J. Chem. Soc. Faraday Trans. II* **73**, 356 (1977).
- [34] E. Lomba, J.-J. Weis, N. G. Almarza, F. Bresme, and G. Stell, *Phys. Rev. E* **49** (1994) 5169.
- [35] N.F. Carnahan and K.E. Starling, *J. Chem. Phys.* **51**, 635 (1969).
- [36] M.P. Allen and D.J. Tildesley *Computer simulation of liquids* Oxford University Press (1987).
- [37] A.M. Ferrenberg and R.H. Swendsen, *Phys. Rev. Lett.* **63**, 1195 (1989).
- [38] B.A. Berg and T. Neuhaus, *Phys. Rev. Lett.* **68**, 9 (1992).
- [39] N.B. Wilding. *Am. J. Phys.* **69**, 1147 (2001).

- [40] C. Borgs and R. Kotecky, Phys. Rev. Lett. **68**, 1734 (1992).
- [41] M. M. Tsypin and H. W. J. Blöte, Phys. Rev. E **62**, 73 (2000).
- [42] I.D. Lawrie and S. Sarbach, in *Phase Transition and Critical Phenomena*, edited by C. Domb and J.L. Lebowitz, Vol. 9 (Academic Press, London) 1984.
- [43] J.M. Tavares, M.M. Telo da Gama, P.I.C. Teixeira, J.-J. Weis, and M.J.P. Nijmeijer, Phys. Rev. E **52**, 1915 (1995); M.J.P. Nijmeijer and J.-J. Weis, Phys. Rev. Lett. **75**, 2887 (1995); M.J.P. Nijmeijer and J.-J. Weis, Phys. Rev. E **53**, 591 (1996); J.-J. Weis, M.J.P. Nijmeijer, J.M. Tavares, and M.M. Telo da Gama, Phys. Rev. E **55**, 436 (1997).
- [44] P.C. Hemmer and D. Imbro, Phys. Rev. A **16**, 380 (1977); W. Fenz, R. Folk, I.M. Mryglod, and I.P. Omelyan, Phys. Rev. E **68**, 061510-1 (2003); I.P. Omelyan, I.M. Mryglod, R. Folk, and W. Fenz, Phys. Rev. E **69**, 061506-1 (2004); I.P. Omelyan, W. Fenz, I.M. Mryglod, and R. Folk, Phys. Rev. Lett. **94**, 045701-1 (2005).
- [45] B. Groh and S. Dietrich, Phys. Rev. E **50**, 3814 (1994); B. Groh and S. Dietrich, Phys. Rev. Lett. **72**, 2422 (1994); *ibid.* **74**, 2617 (1997).
- [46] J.M. Tavares, M.M. Telo da Gama, P.I.C. Teixeira, J.-J. Weis, and M.J.P. Nijmeijer, Phys. Rev. E **52**, 1915 (1995).
- [47] M Buzzacchi, P. Sollich, N.B. Wilding and M. Mller, Phys. Rev. E **73**, 046110 (2006).
- [48] J. Köfinger, Diploma-thesis (Technische Universität Wien, 2004, unpublished).

van Konynenburg and Scott		Tavares <i>et al.</i>	
$\Lambda < 0$	I-A	$\alpha > 1$	no demixing
$\Lambda > 0$	II-A	$\alpha < 1$	I
	II-A*		II- $\alpha$
	III-A*		II- $\beta$
	III-HA		III
	not classified		IV

TABLE I: Correspondence between the types of binary symmetric mixtures classified by van Konynenburg and Scott (see Figs. 1 and 38 of [1]) and the types I, II, III, and IV introduced by Tavares *et al.* [46]. Types II- $\alpha$  and II- $\beta$  are subtypes of type II that are described in more detail in [48].  $\Lambda$  and  $\alpha$  are parameters that characterize the relative strength of the mixed interaction of the binary (size-)symmetrical mixture. Note that this table was already published in [22].

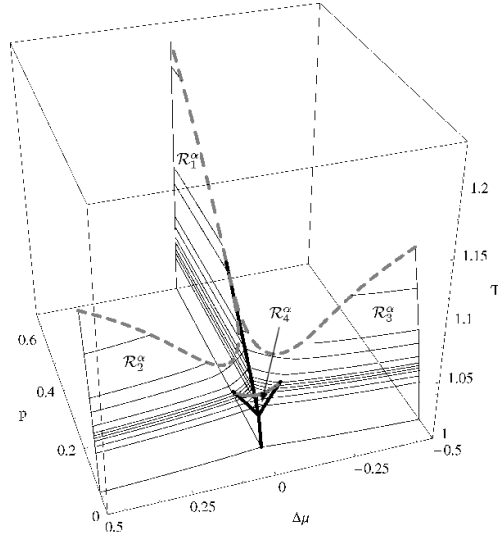


FIG. 1: MSA results for the type  $\alpha$  phase diagram of the binary symmetrical mixture ( $\delta = 0.67$ ) considered in this study in  $(T, p, \Delta\mu)$ -space. Symbols: thin full lines – isothermal coexistence lines, grey full thick line – critical line  $c_4^\alpha$  passing through the LV critical point, grey dashed thick lines – critical lines ( $c_1^\alpha$ ,  $c_2^\alpha$ , and  $c_3^\alpha$ ) passing through the tricritical point, black thick lines – triple lines  $t_i^\alpha$ ,  $i = 1, \dots, 4$ .

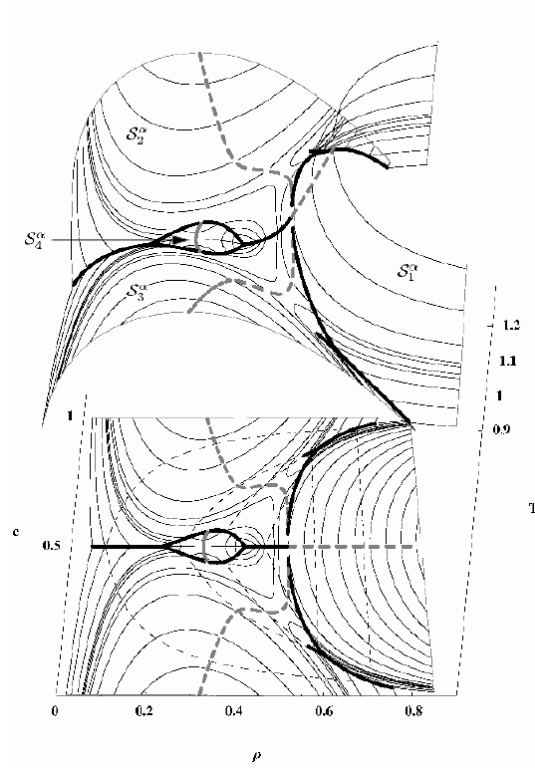


FIG. 2: MSA results for the type  $\alpha$  phase diagram of the binary symmetrical mixture ( $\delta = 0.67$ ) considered in the study in  $(T, \rho, c)$ -space and its projection onto the  $(\rho, c)$ -plane. Symbols: thin full lines – isothermal coexistence lines, dashed thin lines – tie lines, grey full thick line – critical line  $c_4^\alpha$  passing through the LV critical point of field-free case, grey dashed thick lines – critical lines ( $c_1^\alpha$ ,  $c_2^\alpha$ , and  $c_3^\alpha$ ) passing through the tricritical point of the field-free case, black thick lines – triple lines  $t_i^\alpha$ ,  $i = 1, \dots, 4$ .

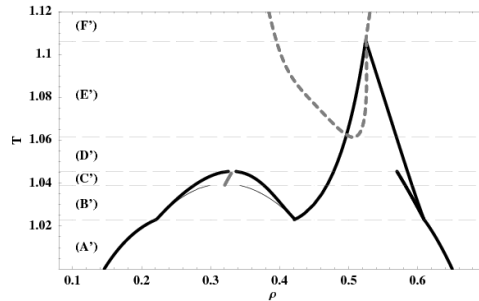


FIG. 3: MSA results for the type  $\alpha$  phase diagram of the binary symmetrical mixture ( $\delta = 0.67$ ) considered in the study, projected onto the  $(T, \rho)$ -plane. Dashed thin lines separate ranges A' to F' (see text). Line symbols see Figs. 1 and 2; in addition: thin line – azeotropic (i.e., field-free coexistence) line.



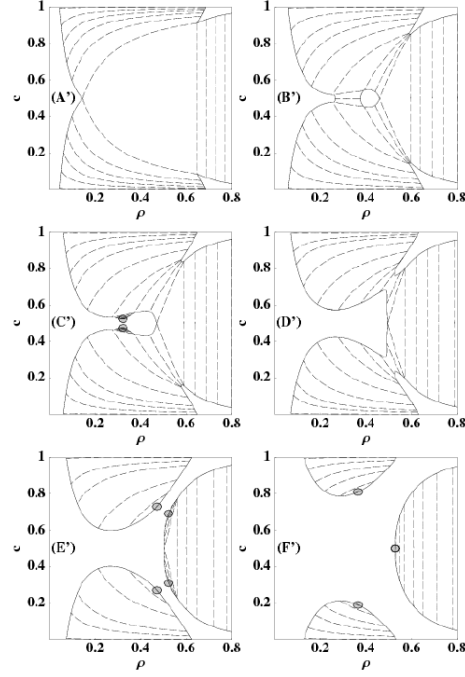


FIG. 4: Six different panels display MSA results for the type  $\alpha$  phase diagram of the binary symmetrical mixture ( $\delta = 0.67$ ) considered in the study, projected onto the  $(\rho, c)$ -plane. The six panels labeled A' to F' show isothermal cuts at the temperatures  $T = \{1, 1.035, 1.041, 1.06, 1.07, 1.15\}$  and correspond to the six temperature ranges indicated in Fig. 3.

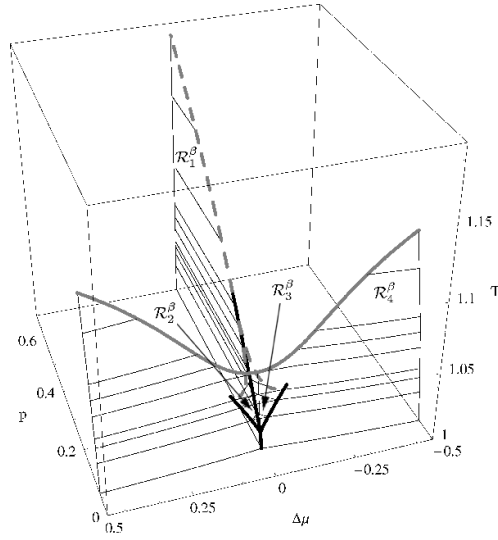


FIG. 5: MSA results for the type  $\beta$  phase diagram of the binary symmetrical mixture ( $\delta = 0.69$ ) considered in this study in  $(T, p, \Delta\mu)$ -space. Symbols: thin full lines – isothermal coexistence lines, grey full thick line – critical line  $c_4^\beta$  passing through the LV critical point, grey dashed thick lines – critical lines ( $c_1^\beta$ ,  $c_2^\beta$ , and  $c_3^\beta$ ) passing through the tricritical point, black thick lines – triple lines  $t_i^\beta$ ,  $i = 1, \dots, 4$ .

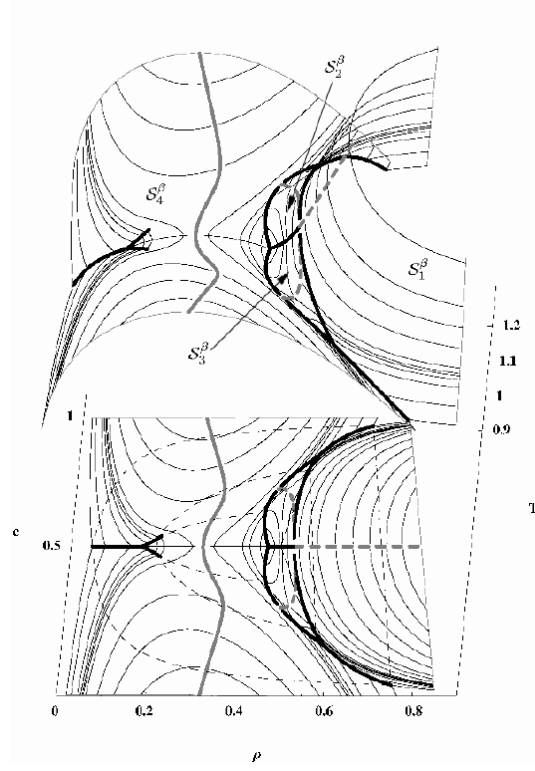


FIG. 6: MSA results for the type  $\beta$  phase diagram of the binary symmetrical mixture ( $\delta = 0.69$ ) considered in the study in  $(T, \rho, c)$ -space and its projection onto the  $(\rho, c)$ -plane. Symbols: thin full lines – isothermal coexistence lines, dashed thin lines – tie lines, grey full thick line – critical line  $c_4^\beta$  passing through the LV critical point of field-free case, grey dashed thick lines – critical lines ( $c_1^\beta$ ,  $c_2^\beta$ , and  $c_3^\beta$ ) passing through the tricritical point of the field-free case, black thick lines – triple lines  $t_i^\beta$ ,  $i = 1, \dots, 4$ .

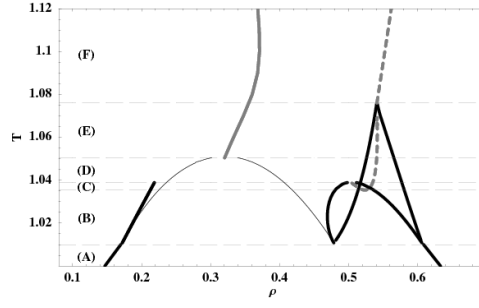


FIG. 7: MSA results for the type  $\beta$  phase diagram of the binary symmetrical mixture ( $\delta = 0.69$ ) considered in the study projected onto the  $(T, \rho)$ -plane. Dashed thin lines separate ranges A to F (see text). Line symbols see Figs. 5 and 6; in addition: thin line – azeotropic (i.e., field-free coexistence) line.

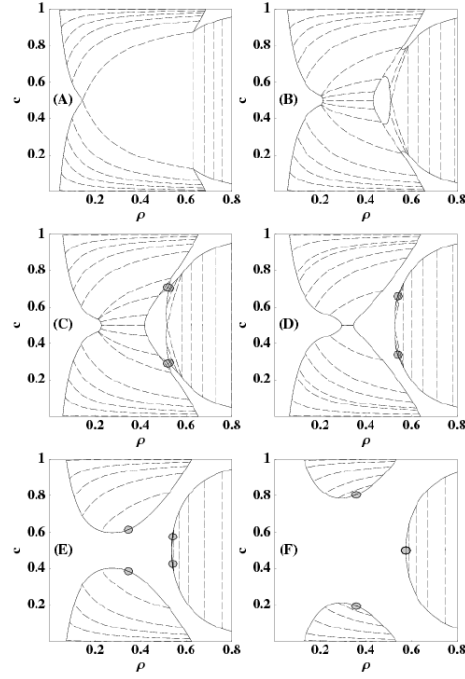


FIG. 8: Six different panels display MSA results for the type  $\beta$  phase diagram of the binary symmetrical mixture ( $\delta = 0.69$ ) considered in the study, projected onto the  $(\rho, c)$ -plane. The six panels labeled A to F show isothermal cuts at the temperatures  $T = \{1, 1.03, 1.036, 1.05, 1.07, 1.15\}$  and correspond to the six temperature ranges indicated in Fig. 7.

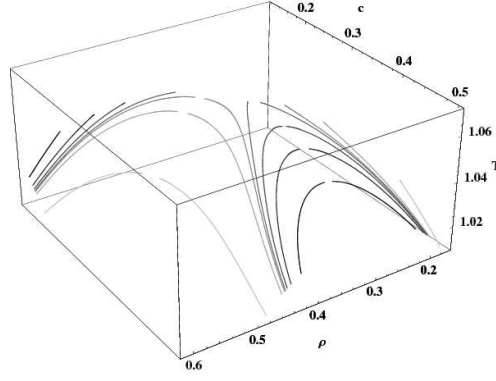


FIG. 9: View of the triple lines  $t_3^\alpha$  and  $t_3^\beta$  from the equimolar plane ( $c = 1/2$ ) in  $(T, \rho, c)$ -space for seven different values of  $\delta = \{0.67, 0.675, 0.677, 0.678, 0.6785, 0.68, 0.69\}$  denoted in gray scales from light gray to black.

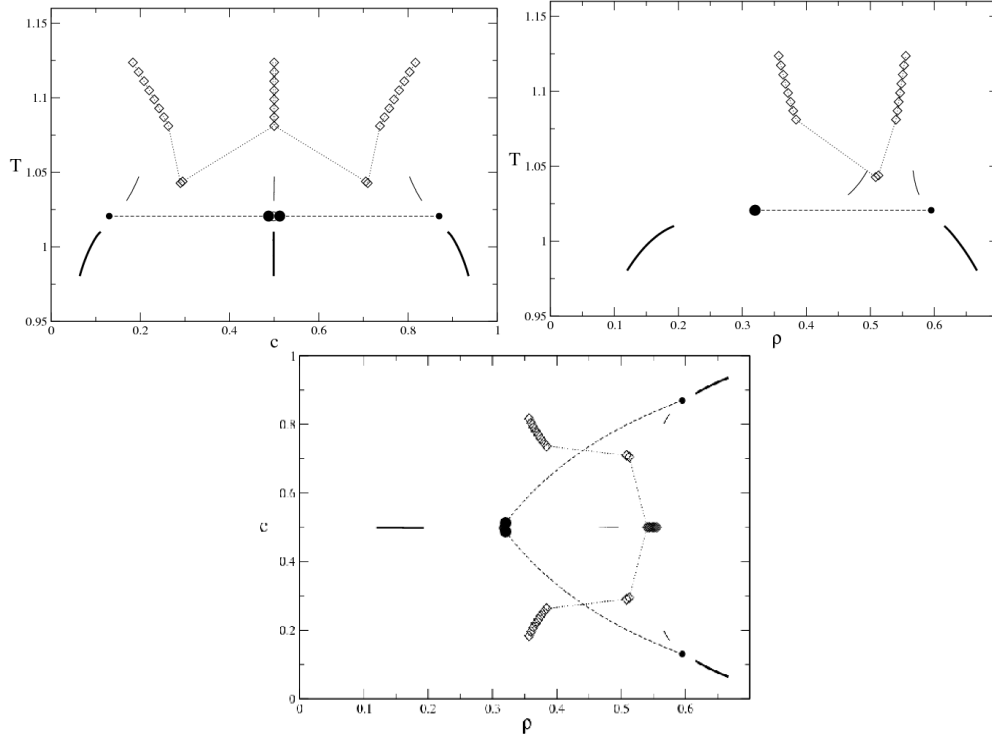


FIG. 10: Projections of the phase diagram measured by simulation for  $\delta = 0.66$  (a)  $(T, c)$ -plane. (b)  $(T, \rho)$ -plane (c)  $(c, \rho)$ -plane. Solid lines are first order phase boundaries. Thin solid coexistence lines are influenced by finite-size effects and serve as a guide to the eye. Diamonds represent points on critical lines passing through the field-free tricritical point, whereas circles represent points of the critical line passing through the field-free LV critical point. Critical points that belong to the same critical line are connected via dotted lines. Large filled symbols represent CEPs and small filled symbols the corresponding spectator phases. Tie lines that connect the spectator phase with the CEP are shown as dashed lines.

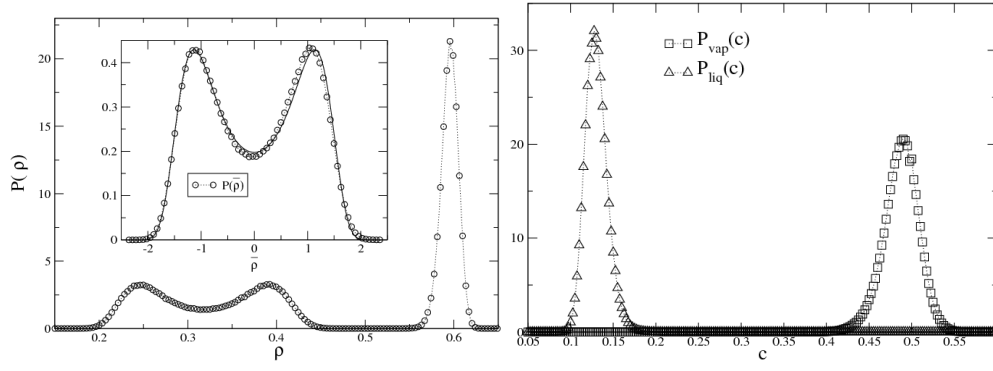


FIG. 11: Critical end point data for  $\delta = 0.66$ . (a) the density distribution  $P(\rho)$ ; also shown (inset) is the accord between  $P(\rho)$  for the critical phase and the appropriately scaled universal Ising fixed point form (see text). (b) the concentration distribution  $P(c)$ .

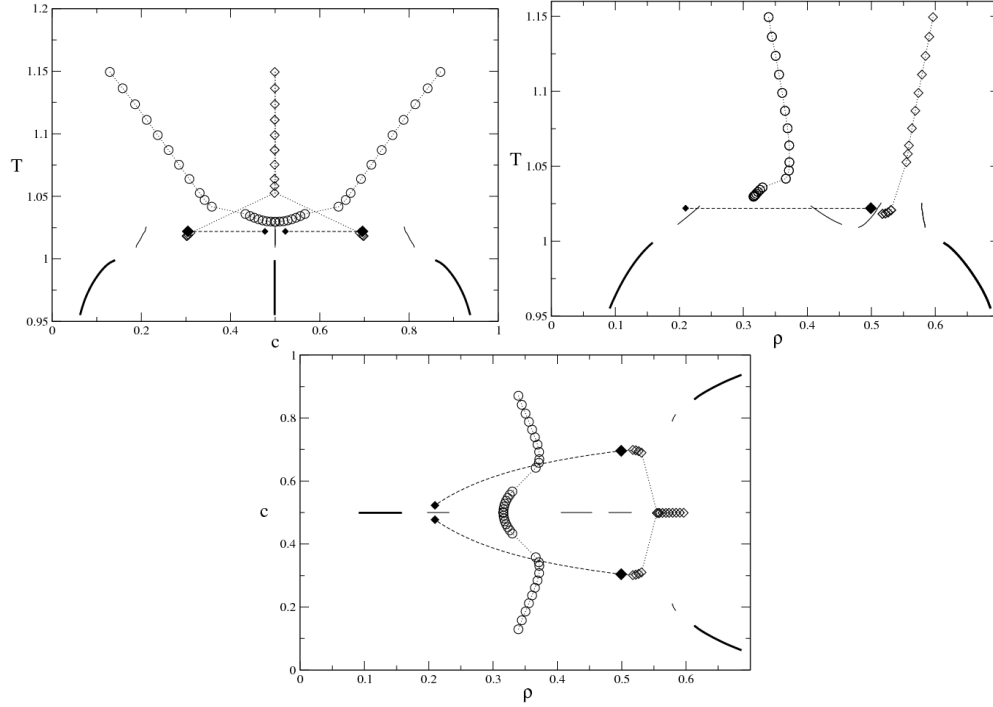


FIG. 12: Projections of the measured phase diagram for  $\delta = 0.68$  (a)  $(T, c)$ -plane, (b)  $(T, \rho)$ -plane, and (c)  $(c, \rho)$ -plane. For an explanation of symbols, see Fig. 10.

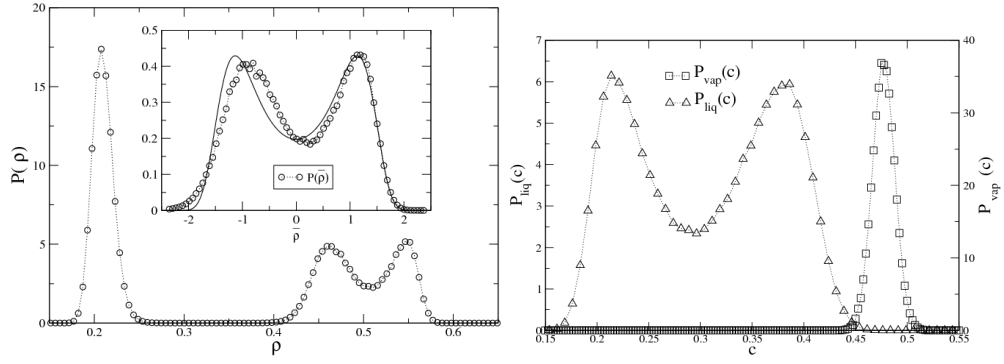


FIG. 13: Critical end point data for  $\delta = 0.68$ . (a) the density distribution  $P(\rho)$ ; also shown (inset) is the accord between  $P(\rho)$  for the critical phase and the appropriately scaled universal Ising fixed point form (see text). (b) the concentration distribution  $P(c)$ , where for clarity the two peaks are presented on different scales.